Journal of Alloys and Compounds 509 (2011) 9946–9950

Contents lists available at ScienceDirect

Journal of Alloys and Compounds

journal homepage: www.elsevier.com/locate/jallcom

Upconversion luminescence properties of Tm^{3+}–Yb^{3+} co-doped titania–zirconia composites nanocrystals

Junjie Lu, Deqiang Wang*, Hailong Wang

Key Laboratory for Ultrafine Materials of Ministry of Education, School of Materials Science and Engineering, East China University of Science and Technology, Shanghai 200237, PR China

ARTICLE INFO

Article history:
Received 21 December 2010
Received in revised form 28 July 2011
Accepted 30 July 2011
Available online 4 August 2011

Keywords:
Upconversion emissions
Titania–zirconia composites
Tm^{3+}–Yb^{3+} rare earth

ABSTRACT

Tm^{3+}–Yb^{3+} co-doped titania–zirconia composites were synthesized by co-precipitation method with aqueous ammonia as precipitator. Time evolution of upconverted emission of thulium in $ZT_{0.4}$–$Tm_{0.01}Yb_{0.04}$ (40%ZrO_2–60%TiO_2–1%Tm^{3+}–4%Yb^{3+}) demonstrated $ZT_{0.4}$ to be a promising matrix in the field of upconversion luminescence. Raman spectrum shows low phonon energy (800 cm^{-1}) of $ZT_{0.4}$ ensuring a fluent phonon transition process. The luminescent properties were investigated by photoluminescence spectra. Strong blue and red upconversion emissions could be observed which were attributed to $^1G_4$–$^3H_6$, $^3F_2$–$^3H_6$, $^1G_4$–$^3F_4$ transitions, respectively.

1. Introduction

Glass host systems (such as tellurite and bismuthate glasses [1,2]) for upconversion (UC) luminescence have been widely studied because they have low phonon energies. But their applications are greatly restricted due to poor chemical stability and mechanical properties. Moreover, they are not suitable for industrial production on account of environmental contamination. On the other hand, ceramics and nanocrystals have attracted a great deal of interest in recent years thanks to their good physical, chemical, mechanical and ultraviolet radio-resistance stability. Ma et al. [3] achieved intense blue photoluminescence from single crystalline hexagonal phase $NaYF_4$ nanorods. Nikifor and Maciel [4] found valuable blue shift in Nd^{3+} doped yttrium oxide powders pumped by pulsed red laser. Hou et al. [5] reported $Tm^{3+}/Er^{3+}/Yb^{3+}$ tri-doped Y_2O_3 transparent ceramic that could present various colors of upconversion luminescence by varying the concentration of rare earth. Some other brand new ceramics like NBT ($Na_{1/2}Bi_{1/2}TiO_3$) [6], $Gd_4O_3F_6$ [7], cubic-structure Ba_2YbF_7 [8] have also been reported and demonstrated to be good candidates for upconversion in sophisticated applications such as biomedical detection, optical imaging, solar energy converters, etc.

Luminescence properties of Tm^{3+} doped UC systems can also be found in literatures, such as transparent ceramic [9], $NaYF_4$ [10], YVO_4 [11] matrix, etc. As one of the most important rare earth ions, Tm^{3+} is often co-doped with other rare earth [12,13] ions like Yb^{3+} to achieve the energy upconversion [14]. In particular, well-known efficient energy transfer processes from Yb^{3+} to two Tm^{3+} ions [15] due to high absorption cross-section transition of Yb^{3+} ions, $^2F_{7/2} \rightarrow {}^2F_{5/2}$ excited at 980 nm, give rise to the required visible RGB up-conversion emissions. Also, Tm^{3+}–Yb^{3+} co-doped UC system will present many other valuable characteristics in different kinds of matrix [16,17].

In our previous report [18], we presented titania–zirconia composite ($ZT_{0.4}$) as a new host system. When Er^{3+}–Yb^{3+} were co-doped, strong green and red upconversion emissions were observed. We optimized the composition of the host system and discussed the excited state absorption (ESA) process by 980 nm excitation. In this work, Tm^{3+}–Yb^{3+} co-doped titania–zirconia composite synthesized by co-precipitation method is reported. Influences of sintering temperature and dopant concentration on the up-conversion luminescence are explored in detail. Raman spectrum shows low phonon energy (800 cm^{-1}) of $ZT_{0.4}$. Strong blue and red emissions can be detected under 980 nm laser excitation. So, we can achieve simultaneously controllable red, green, and blue (RGB) emissions when co-dope certain rare-earth element in $ZT_{0.4}$. It is of great significance because the $ZT_{0.4}$ may serve as a new ceramic matrix for upconversion and attract wide attention in the field of luminescence.

2. Experimental

Tm^{3+} and Yb^{3+} ions were co-doped in the $ZT_{0.4}$ (ZrO_2–TiO_2) host system, samples were synthesized by co-precipitation method. Analytical grade $TiCl_4$, $ZrOCl_2 \cdot 8H_2O$, $Tm(NO_3)_3 \cdot 6H_2O$ and $Yb(NO_3)_3 \cdot 6H_2O$ were dissolved in de-ionized water and mixed homogeneously. The mixture was stirred in a beaker for 0.5 h which was then added dropwise into ammonia with quick stirring. The precipitates were subsequently

---

* Corresponding author. Tel.: +86 21 64252842; fax: +86 21 64252842.
E-mail address: Derek_wang@ecust.edu.cn (D. Wang).

0925-8388/$ – see front matter © 2011 Elsevier B.V. All rights reserved.
doi:10.1016/j.jallcom.2011.07.104

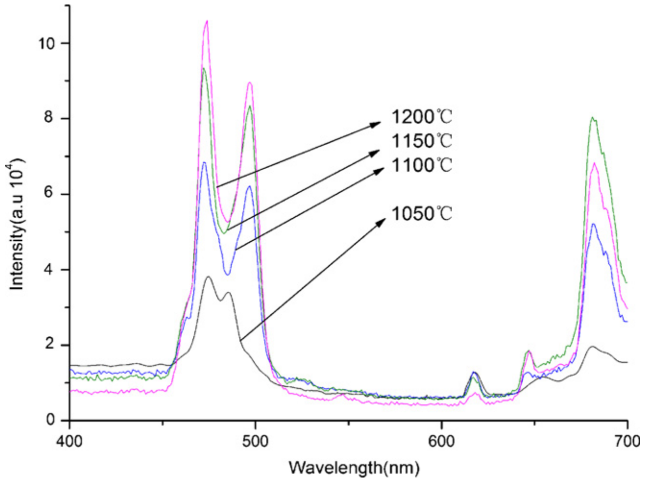

Fig. 1. Upconversion luminescence spectra of $ZT_{0.4}$–$Tm_{0.01}Yb_{0.04}$ sintered at different temperature.

dried at 80 °C for 24 h after filtrated and washed twice with de-ionized water, 1 h each time, to get rid of the impurity ions. The grinded powders were sintered at different temperature (1050 °C, 1100 °C, 1150 °C, 1200 °C) for 2 h.

Crystal phases of sintered samples were identified by powder X-ray diffraction (XRD). The XRD patterns of the different samples were recorded by BRUKER D8 Focus X-ray powder diffractometer with Cu Kα (λ = 0.15 nm) radiation generated at 40 kV/40 mA and the 2θ range was varied between 20° and 80°. The emission spectra of samples were detected by Fluorolog-3-P UV–vis-NIR fluorescence spectrophotometer (Jobin Yvon, France) which could work with a 980 nm semiconductor solid pulsed laser (laser power: 500 mW; pulse width: 1–600 μs; repetition rate: 1–30 kC). The luminescence decay was performed by Tektronix TDS 3025 digital oscilloscope, following 980 nm short pulse excitation. The Raman spectrum was recorded on a FT-Raman spectrophotometer (Invia Raman Microscope, RENISHAW) within the range of 100–1200 cm^{-1}. Thermal analyses were detected from room temperature to 1000 °C by simultaneous thermal analyzer (STA 449 F1, NETZSCH).

3. Results and discussion

Fig. 1 shows the up-conversion luminescence spectra of $ZT_{0.4}$–$Tm_{0.01}Yb_{0.04}$ sintered at different temperature. Emission bands can be observed at blue (around 475 nm) and red (around 690 nm) regions and it is clear that the emission intensity increases with the increasing sintering temperature.

The pattern of thermal analysis (TG and DTA) is presented in Fig. 2. Clearly, about 55% of the total weight of precursor lost during the sintering process (due to the H_2O, NH_3 and NO_x release). But the weight was stable when the sintering temperature was higher than 670 °C, which was much lower than the forming point of $ZrTiO_4$. So, the increase of luminescence intensity was possibly on account of the change of subtle phase of $ZT_{0.4}$ at high sintering temperature. From XRD patterns shown in Fig. 3, evolution of subtle phase change of $ZT_{0.4}$ corresponding to different sintering temperature is presented. At 1050 °C, $ZrTiO_4$, TiO_2 and ZrO_2 were basically formed. But their characteristic diffraction peaks are not sharp enough to demonstrate integrated phases. So, upconversion emission intensities of the sample are very low. When the temperature was above 1100 °C, all diffraction peaks became shaper and the emissions of the samples in blue and red region were enhanced. At 1200 °C, peaks of $ZrTiO_4$ strengthened while those of ZrO_2 and TiO_2 weakened, indicating that $ZrTiO_4$ become dominant in the $ZT_{0.4}$ matrix.

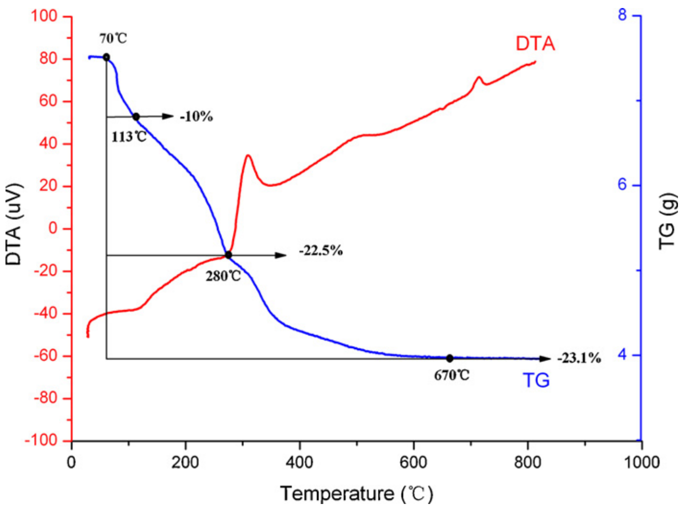

Fig. 2. Thermal analysis of $ZT_{0.4}$ matrix.

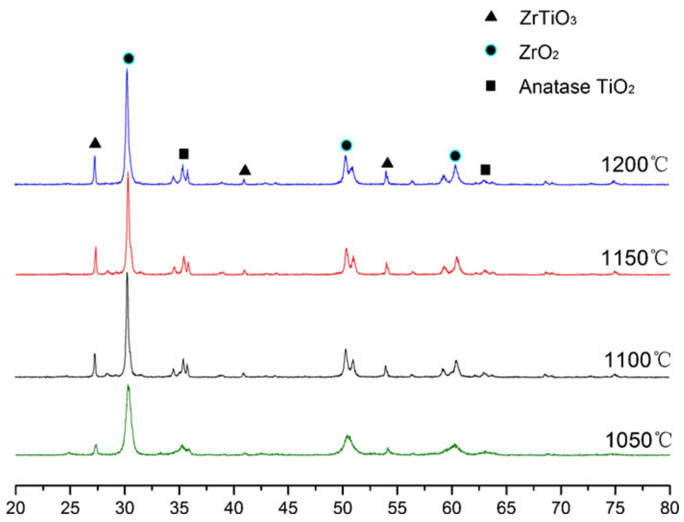

Fig. 3. Powder X-ray patterns of $ZT_{0.4}$ matrix sintered at different temperature.

In our previous report [18], we explored the effect of matrix composition ZT_x (x = 0, 0.2, 0.4, 0.5, 0.6, 0.7, 0.8, 1) on the crystal formation. It was found that when ZrO_2 was dominant, formation of $ZrTiO_4$ crystal phase became difficult. On the other hand, dominant TiO_2 favored a metastable crystalline structure of anatase TiO_2. Also, the sintering temperature could influence the crystal structure of the matrix greatly so as to exert remarkable effects on upconversion luminescence properties.

Fig. 4 shows the Raman spectra of $ZT_{0.4}$–$Tm_{0.01}Yb_{0.04}$ sintered at 1000 °C and 1200 °C. It is found that Zr–O vibration is dominant at 1000 °C because monoclinic ZrO_2 can be formed at about 950 °C which is lower than the forming point of TiO_2 and $ZrTiO_4$. When sintered at 1200 °C, Zr–O vibration weakened while Ti–O vibration strengthened, demonstrating the forming of TiO_2 and $ZrTiO_4$ at relatively high sintering temperature, which is in accordance with the XRD pattern. From another point of view, radius of Zr (2.2 Å) is larger than Ti (2.0 Å), while the radius of Yb and Tm is about 2.4 Å. Thus, rare earth elements may have the priority to substitute for Zr at low sintering temperature and then, the whole $ZrTiO_4$ lattice at high sintering temperature. Different substituted positions may benefit certain bands of emission. ZrO_2 and TiO_2 phases impede the fully doping of rare earth, they are not favorable in the multi-component matrix. When ZrO_2–TiO_2 ($ZrTiO_4$) eutectic formed at high temperature, the up-conversion emissions could be successfully enhanced.

The influence of dopant concentration on the up-conversion luminescence was also explored. Up-conversion luminescence spectra of samples 1–5 with different mole ratio of Tm/Yb are presented in Fig. 5. Two main distinct up-conversion emission bands

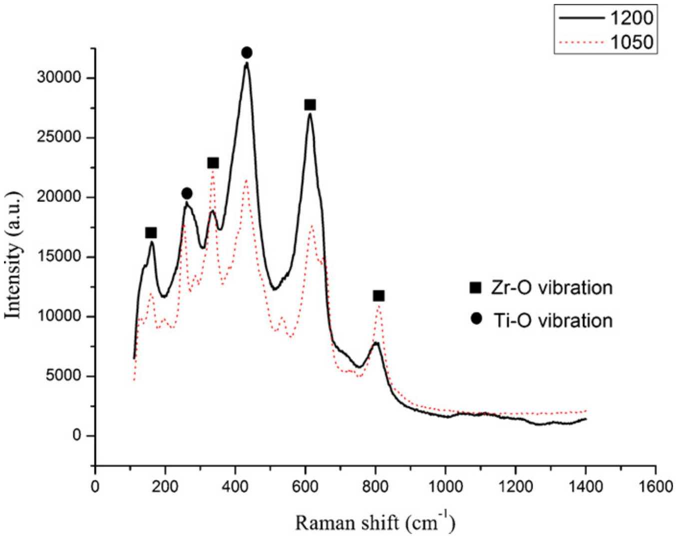

Fig. 4. Raman spectra of $ZT_{0.4}$–$Tm_{0.01}Yb_{0.04}$ sintered at different sintering temperature.

around 470–500 nm and 650–700 nm were detected where the major emission band was around 475 nm. When 0.5% Yb^{3+} (sample 1) was doped, basically no emission band could be found (see Fig. 6). But with the increasing concentration of doped Yb^{3+}, the emission intensity strengthened. The $ZT_{0.4}$–$Tm_{0.01}Yb_{0.04}$ (sample 4) achieved the highest emission intensity.

We can come to a basic conclusion that Yb^{3+} ion plays an important role in the $ZT_{0.4}$ upconversion system. When the system was pumped by 980 nm laser excitation, Yb^{3+} ion accepted energies and acted as the "energy source" in up-conversion processes. Tm^{3+} ion offered the energy orbits which transferred phonon energies. So, Yb^{3+} ion was the "bridge" that accepted the energy from the activator and transferred to the Tm^{3+} energy orbits. In this way, low concentration of Tm^{3+} satisfied the up-conversion process while a respectively high concentration of Yb^{3+} could greatly enhance the intensity of emission.

The Raman spectrum of the $ZT_{0.4}$ matrix is presented in Fig. 7. Absorption bands at 160 cm^{-1}, 336 cm^{-1}, 616 cm^{-1} and 800 cm^{-1} are assigned to the Zr–O vibration while 256 cm^{-1} and 444 cm^{-1} are assigned to the Ti–O vibration. Compared with other popular matrix for upconversion listed in Fig. 7, the maximum phonon energy of $ZT_{0.4}$ is also very low (about 800 cm^{-1}), which benefits the multi-phonon relaxation rate of the rare earth ions. Time evolution of up-converted emission (475 nm) of thulium ($^1G_4$–$^3H_6$) in the $ZT_{0.4}$–$Tm_{0.01}Yb_{0.04}$ excited with a pulse at 980 nm is present in Fig. 8. The luminescence intensity rose initially, attained a max-

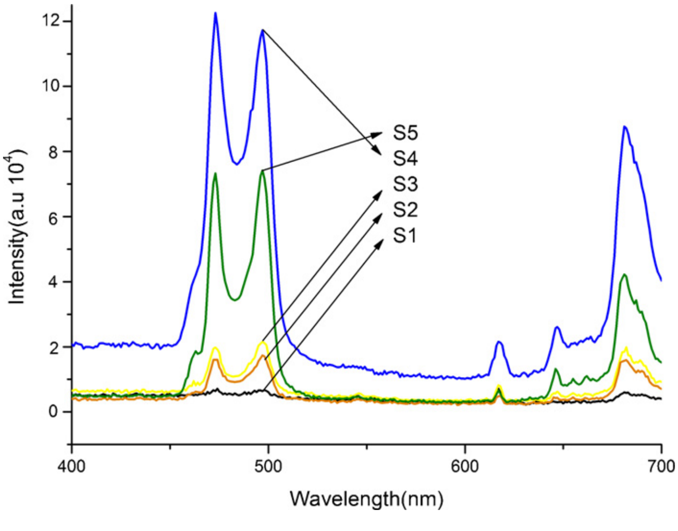

Fig. 5. Upconversion luminescence spectra of samples 1–5 (S1: $ZT_{0.4}$–$Tm_{0.01}Yb_{0.005}$, S2: $ZT_{0.4}$–$Tm_{0.01}Yb_{0.01}$, S3: $ZT_{0.4}$–$Tm_{0.01}Yb_{0.02}$, S4: $ZT_{0.4}$–$Tm_{0.01}Yb_{0.04}$, and S5: $ZT_{0.4}$–$Tm_{0.01}Yb_{0.06}$).

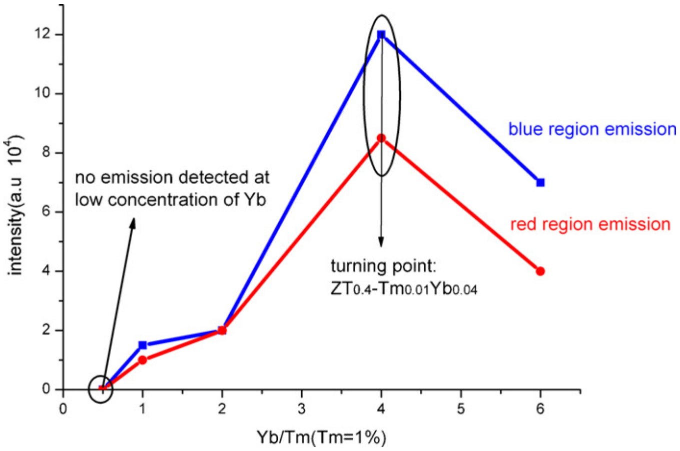

Fig. 6. Intensity variation of the luminescence spectra of samples 1–5.

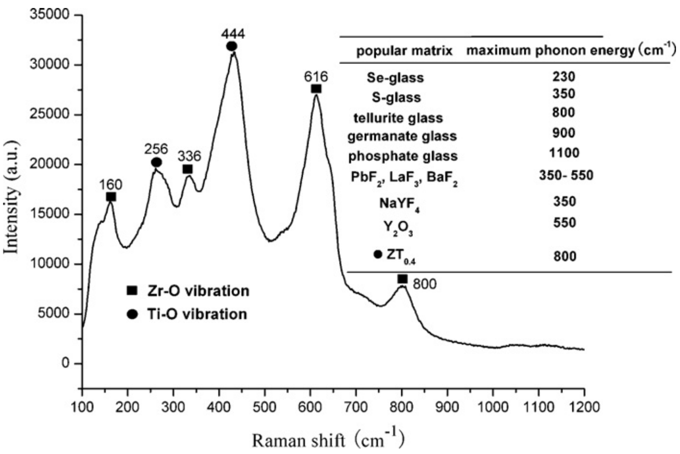

Fig. 7. Raman spectra of $ZT_{0.4}$ matrix (compared with other popular matrix).

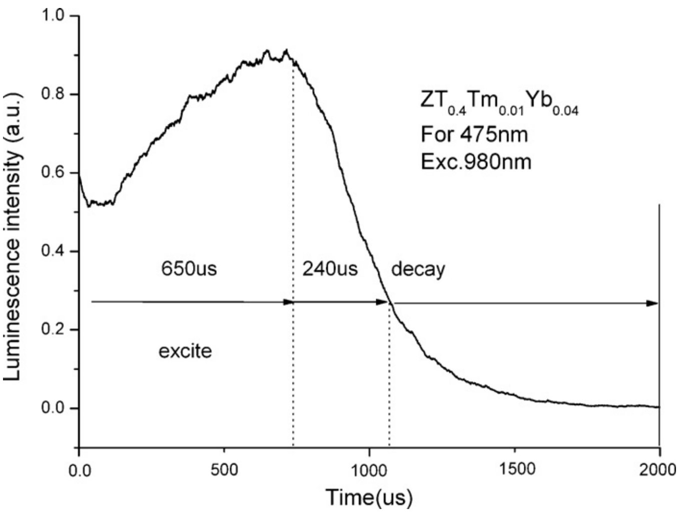

Fig. 8. Time evolution of upconverted emission (475 nm) of thulium $^1G_4$–$^3H_6$ in the $ZT_{0.4}$–$Tm_{0.01}Yb_{0.04}$, excited with a pulse at 980 nm.

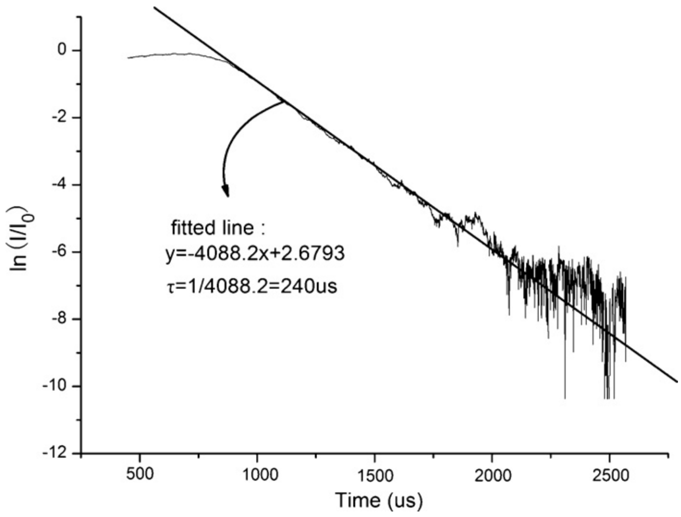

Fig. 9. Decay curve of the $^1G_4$–$^3H_6$ emission of Tm^{3+} in $ZT_{0.4}$.

imum at 650 us receiving the excitation pulse, and then decayed slowly. Also, through the decay curve of $^1G_4$–$^3H_6$ of Tm^{3+} presented in Fig. 9, the life time of the main fluorescence (475 nm, $^1G_4$–$^3H_6$) was calculated to be 240 μs which is consistent with the decay time presented in Fig. 8.

Combined with Fig. 10 (thin lines with arrow indicate the excitation processes, thick lines indicate the emission processes), we can understand the mechanism of $ZT_{0.4}$ co-doped system. Time dependence of the luminescence intensity is controlled by lifetime of levels involved in the complex energy transfer processes, which is supposed to proceed as follows.

$$\text{Absorption}: Yb^{3+}(^2F_{7/2}) + \text{photons} \rightarrow Yb^{3+}(^2F_{5/2})$$

Excitation processes:

a: $Yb^{3+}\ (^2F_{5/2}) + Tm^{3+}\ (^3H_6) \rightarrow Yb^{3+}\ (^2F_{7/2}) + Tm^{3+}\ (^3H_5) + \text{phonons}$
b: $Tm^{3+}\ (^3H_5) \rightarrow Tm^{3+}\ (^3F_4) + \text{phonons}$
c: $Yb^{3+}\ (^2F_{5/2}) + Tm^{3+}\ (^3F_4) \rightarrow Yb^{3+}\ (^2F_{7/2}) + Tm^{3+}\ (^3F_2) + \text{phonons}$
d: $Tm^{3+}\ (^3F_2) \rightarrow Tm^{3+}\ (^3H_4) + \text{phonons}$
e: $Yb^{3+}\ (^2F_{5/2}) + Tm^{3+}\ (^3H_4) \rightarrow Yb^{3+}\ (^2F_{7/2}) + Tm^{3+}\ (^1G_4) + \text{phonons}$
f: $Tm^{3+}\ (^1G_4) \rightarrow Tm^{3+}\ (^3F_2) + \text{phonons}$

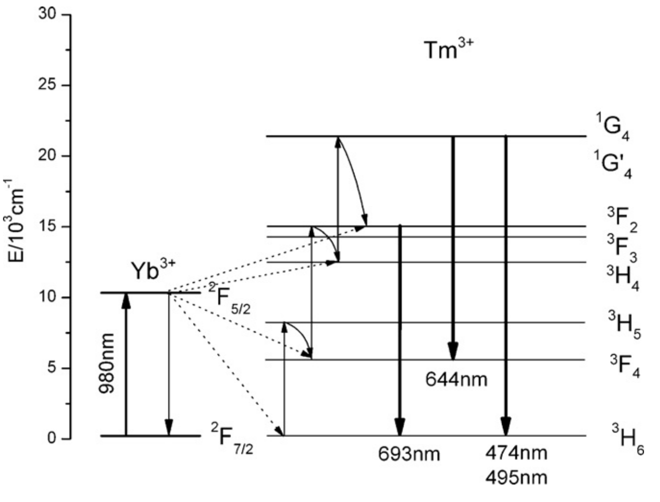

Fig. 10. Energy level diagram of Tm^{3+} and Yb^{3+} ions and upconversion mechanism.

Emission processes:

a: $Tm^{3+}\ (^3F_2) \rightarrow Tm^{3+}\ (^3H_6) + h\nu(693\,\text{nm})$
b: $Tm^{3+}\ (^1G_4) \rightarrow Tm^{3+}\ (^3F_4) + h\nu(644\,\text{nm})$
c: $Tm^{3+}\ (^1G_4) \rightarrow Tm^{3+}\ (^3H_6) + h\nu(474\,\text{nm})$
c′: $Tm^{3+}\ (^1G'_4) \rightarrow Tm^{3+}\ (^3H_6) + h\nu(495\,\text{nm})$

The step of absorption is the "engine" of all the process afterwards. The excited state Yb^{3+} ($^2F_{5/2}$) offer phonon energies to Tm^{3+} ions and excite them up to their corresponding excited level. Excitation processes a, c, and e show that Tm^{3+} ions are excited to higher energy level after absorbing phonon energy from Yb^{3+} ($^2F_{5/2}$), then Yb^{3+} ions return back to ground state level Yb^{3+} ($^2F_{7/2}$). Meanwhile, the excited Tm^{3+} ions are unstable. Excitation processes b, d, and f show that excited Tm^{3+} ions fall back to relatively lower energy levels, releasing certain amounts of phonon energies.

Yb^{3+} sensitized Tm^{3+} ion is an efficient system for near-infrared to visible frequency upconversion. The strong blue emission around 495 nm (475 nm) easily seen by naked eye is assigned to the $^1G_4 \rightarrow {}^3H_6$ transition of Tm^{3+} ions. Weak red emission around 693 nm is attributed to the $^3F_2 \rightarrow {}^3H_6$ transition. Under 980 nm laser excitation, three-step ET (energy transfer) can successively take place between a Tm^{3+} ion and three excited Yb^{3+} ions nearby, corresponding to excitation processes a, c, and e. Then, the Tm^{3+} ions decay radiatively to the $^3H_6$ ground state and the $^3F_4$ metastable state generating strong blue and weak red emissions around 495(475) nm and 644 nm from the $^1G_4$ level, respectively (corresponding to emission processes b and c).

4. Conclusions

Tm^{3+}–Yb^{3+} co-doped titania–zirconia composites were synthesized by a homogeneous precipitation method. $ZT_{0.4}$ was demonstrated to be a nice host system in the field of up-conversion luminescence thanks to its low phonon energy (800 cm^{-1}) and decay rate. Blue and red region emissions were observed from the up-conversion luminescence spectra under 980 nm laser excitation at room temperature. Doping 1%Tm^{3+}–4%Yb^{3+} in $ZT_{0.4}$ matrix was proved to be the best concentration for blue and red region emission. Sintering temperature also exerted remarkable effect on up-conversion luminescence, a high sintering temperature effectively strengthen the luminescence intensity.

Acknowledgements

This study was supported by Shanghai Leading Academic Discipline Project (B502) and Shanghai Key Laboratory Project (08DZ2230500).

References

[1] M. Celikbilek, A.E. Ersundu, N. Solak, S. Aydin, J. Alloys Compd. 509 (2011) 5646–5654.
[2] K.F. Li, H.Y. Fan, G. Zhang, G.X. Bai, S.J. Fan, J. Alloys Compd. 509 (2011) 3070–3073.
[3] M. Ma, C.F. Xu, L.W. Yang, G.Z. Ren, J.G. Lin, Phys. B 406 (2011) 3256–3260.
[4] Nikifor Rakov, G.S. Maciel, Chem. Phys. Lett. 503 (2011) 124–128.
[5] X.R. Hou, S.M. Zhou, T.T. Jia, H. Lin, H. Teng, J. Alloys Compd. 509 (2011) 2793–2796.
[6] T. Passuello, F. Piccinelli, M. Pedroni, M. Bettinelli, Opt. Mater. 33 (2011) 643–646.
[7] H. Guo, Y.F. Li, D.Y. Wang, W.P. Zhang, M. Yin, L.R. Lou, S.D. Xia, J. Alloys Compd. 376 (2004) 23–27.
[8] C.F. Xu, M. Ma, S.J. Zeng, G.Z. Reng, J. Alloys Compd. 509 (2011) 7943–7947.
[9] X. Li, B. Song, S.C. Xu, J.W. Lu, J. Rare Earths 28 (2010) 194–199.
[10] J.F. Suyver, J. Grimm, M.K. van Veen, D. Biner, K.W. Kramer, H.U. Gudel, J. Lumin. 117 (2006) 1–12.
[11] R. Lisiecki, G. Dominiak-Dzik, T. Łukasiewicz, W. Ryba-Romanowski, J. Mol. Struct. 704 (2004) 323–327.

[12] F.C. Guinhos, P.C. Nobrega, P.A. Santa-Cruz, J. Alloys Compd. 323 (2001) 358–361.

[13] J. Yang, C.M. Zhang, C. Peng, C.X. Li, R.T. Chai, J. Lin, Chem. Eur. J. 15 (2009) 4649–4655.

[14] J. Pisarska, R. Lisiecki, W. Ryba-Romanowski, J. Alloys Compd. 451 (2008) 226–228.

[15] S.F. León-Luis, J. Abreu-Afonso, J. Peña-Martínez, J. Méndez-Ramos, A.C. Yanes, J. del-Castillo, V.D. Rodríguez, J. Alloys Compd. 480 (2009) 706–710.

[16] S.J. Zeng, G.Z. Ren, C.F. Xu, J. Alloys Compd. 509 (2011) 2540–2543.

[17] A.S. Aleksandrovsky, I.A. Gudim, A.S. Krylov, A.V. Malakhovskii, V.L. Temerov, J. Alloys Compd. 496 (2010) L18–L21.

[18] Y.F. Hu, D.Q. Wang, Z.J. Li, J.J. Lu, J.B. Zheng, J. Am. Ceram. Soc. 93 (2010) 374–377.